Laser and Particle Beams (2013), *31*, 427–438.

doi:10.1017/S0263034613000293

Proton acceleration by plasma wakefield driven by an intense proton beam

LONGQING YI, BAIFEI SHEN, LIANGLIANG JI, XIAOMEI ZHANG, WENPENG WANG, JIANCAI XU, YAHONG YU, XIAOFENG WANG, YIN SHI, AND ZHIZHAN XU

State Key Laboratory of High Field Laser Physics, Shanghai Institute of Optics and Fine Mechanics, Chinese Academy of Sciences, Shanghai, China

(RECEIVED 3 December 2012; ACCEPTED 26 March 2013)

Abstract

Plasma wakefield excited by a short TeV-scale proton beam is investigated in the highly nonlinear regime. Analysis of the "bubble" field illustrates that transverse expelling force of the wakefield can be compensated by the attractive force, which originates from the co-propagating electrons within the proton bunch, leading to a collimation effect that stabilizes the beam propagation. The protons located in the beam tail can be well-confined and accelerated forward for a long distance. Two-dimensional simulations show that after a 1-TeV proton bunch propagating through plasma for a distance, several percentages of the protons achieve a remarkable energy gain. This scheme presents a potential that proton beams from conventional accelerators may gain considerable additional energy through plasmas wakefields.

Keywords: Plasma lens effect; Plasma wakefield; Proton acceleration; Self-confinement

1. INTRODUCTION

Highly energetic ion beams colliding with each other offers an important way to discover new particles and furthermore new physics. Nowadays, conventional linear and cyclotron accelerators are able to generate proton beams with energy up to several TeV. The Large Hadron Collider (LHC), allowing two 7 TeV proton beams to impinge with each other, seems to have found the Higgs particle that could explain the origin of mass. On the other hand, the future construction of more powerful accelerators based on conventional method is limited by its enormous expense and occupancy area. Plasma, which can sustain extremely large acceleration gradient (three orders of magnitude higher than achieved in conventional accelerators), exhibits great potential to generate energetic proton/ion beams in table-top size or within a lab. Lots of plasma-based acceleration mechanisms have been proposed, where ultra-intense lasers are mostly employed to excite a strong accelerating field in plasmas, such as the well-known target normal sheath acceleration (TNSA) (Schwoerer *et al.*, 2006; Toncian *et al.*, 2006; Albright *et al.*, 2006; Mora *et al.*, 2003; Snavely *et al.*, 2000; Yin *et al.*, 2006; Poukey *et al.*, 1969; Gaillard *et al.*, 2011), the radiation pressure acceleration (RPA) (Macchi *et al.*, 2005; Liseikina *et al.*, 2007; Qiao *et al.*, 2009; 2010; Liseykina *et al.*, 2008; Robinson *et al.*, 2008; Yan *et al.*, 2008; Zhang *et al.*, 2009; 2007a; 2007b; Ji *et al.*, 2008; 2009), the laser break-out afterburner (BOA) (Yin *et al.*, 2007; Flippo *et al.*, 2007; Albright *et al.*, 2007), and laser-driven wakefield acceleration (Shen *et al.*, 2007; 2009; Zhang *et al.*, 2010). The technique of TNSA is more mature than others, especially in experiments. However, the acceleration distance is short and the laser-proton efficiency is relatively low. Up to present 67.5 MeV is the highest proton energy obtained by TNSA using the 80 J PW Trident Laser (Gaillard *et al.*, 2011). BOA is a mechanism in which laser penetrates to the rear of the target and consequently heats the sheath electrons, which enables the proton acceleration to GeV-level with lower laser intensity compared with TNSA. RPA is a newly developed promising approach attracting more and more interest in recent years. Using intense circularly polarized (CP) laser pulses, protons with energy over 1 GeV may be obtained, which have been demonstrated by lots of particle-in-cell (PIC) simulations (Yan *et al.*, 2009; Qiao *et al.*, 2009; Macchi *et al.*, 2009; Chen *et al.*, 2009; Tripathi *et al.*, 2009; Davis *et al.*, 2009; Eliasson *et al.*, 2009). Recent researches have shown that not only electrons but protons can also gain stable

Address correspondence and reprint requests to: Baifei Shen, State Key Laboratory of High Field Laser Physics, Shanghai Institute of Optics and Fine Mechanics, Chinese Academy of Sciences, Shanghai 201800, China. E-mail: bfshen@mail.shcnc.ac.cn

acceleration in laser-driven wakefield, except that protons are accelerated by the positive electrostatic field in the front of "bubble" (Shen *et al.*, 2007). One uses short CP laser pulses interacting with a micro-target embedded in under-dense high-mass plasma. Protons in the micro-target are first pre-accelerated by the laser radiation pressure and gain considerable initial velocity. Then these protons are more easily trapped and steadily accelerated by the induced wake "bubble" field in the background plasma. PIC simulations show that 76 GeV high-quality quasi-mono-energetic protons (Zhang *et al.*, 2010) can be obtained with this approach. Although a lot of progresses have been made, the energy gain in laser-plasma acceleration is still not comparable with the top conventional accelerators even in simulations. The required laser intensity is also very high (2.14×10^{23} Wcm^{-2} for 76 GeV) compared to currently available laser facilities.

In plasma wakefield acceleration, energetic particle beams have also been proposed to be alternate drivers (Esarey *et al.*, 2009; Rosenzweig *et al.*, 1991; Lotov, 2007; Lee *et al.*, 2000; Wang *et al.*, 2009; Joshi *et al.*, 2002; Blumenfeld *et al.*, 2007; Kallos *et al.*, 2008). An intense electron beam can excite wakefield in a plasma, where background electrons are expelled by the beams rather than laser pulses. In this mechanism, the energy gain of the witness beam cannot be more than $2\sqrt{2}$ times of the driver's energy (Bane *et al.*, 1985). Since protons are able to carry much higher energy than electrons in nowadays' accelerators (CERN, LHC, etc.), it is promising to achieve higher energy gain comparable to state-of-art conventional accelerators by using proton drivers (Caldwell *et al.*, 2009; Lotov, 2010; Xia *et al.*, 2010).

In previous proton-driven plasma wakefield researches, where electron acceleration is mostly concerned, it is found that because background electrons are sucked in toward the propagating axis by the positively charged driver instead of being blown out. Electrons originating from different radii arrive at different times, leading to the "phase mixing" effect. It reduces the amplitude of plasma oscillation, and is considered to be the primary limit to the acceleration field (Lee *et al.*, 2001; Kimura *et al.*, 2011).

Following the laser-driven wakefield scenario mentioned above (Shen *et al.*, 2007; 2009; Zhang *et al.*, 2010), one could naturally infer that proton itself can also be accelerated by a proton-driven wakefield. A few researchers have observed proton energy gaining in the driving beam, though lacking specific explanation (Kumar *et al.*, 2010; Caldwell *et al.*, 2011). In this paper, we propose demonstrably that using an energetic proton beam propagating through an under-dense plasma, protons located in the bunch tail can be stably accelerated by its self-driving wakefield. Unlike electrons, protons are supposed to be expelled by the transverse component of the wakefield. However when the density of the driving beam in 6d phase space $d \propto N/(\gamma^2 \sigma_x \varepsilon \sigma_y^2 \alpha^2)$ is large enough, the driver can propagate for a long distance without apparent divergence owing to the "plasma lens" effect (Chen *et al.*, 1987; Su *et al.*, 1990). This effect allows charged particle beams propagating in plasma to be focused due to plasma electrons shifting. Here N is total number of the drive particles, γ, σ_x, σ_y, ε, and α are the Lorentz factor, longitudinal size, transverse size, longitudinal momentum spread and divergence angle of the drive beam, respectively. Confinement of protons at the tail of a dense driving bunch mainly relies on the co-propagating electrons within the proton bunch, which move with the driver with a lower speed. Discussions in more detail will be shown in Section 3.

For proton beams available in recent accelerators, whose phase space densities are much lower, the "plasma lens" effect alone is not sufficient to confine the whole bunch, so extra quadrupole magnets (Caldwell *et al.*, 2009; Lotov, 2010) are employed. The acceleration of the beams with feasible 6d phase space density will be discussed in Section 4.

As the proton bunch propagates in the plasma, energy is continually transmitted from the main body to the tail until phase slippage occurs. After propagating in plasmas for a few meters, the energy of some protons could be considerably increased.

2. LONGITUDINAL WAKEFIELDS GENERATED BY A PROTON BEAM

As a charged beam propagates in a plasma, the plasma electrons will respond to the extra charge and oscillate at plasma frequency $\omega_p = \sqrt{4\pi n_0 e^2/m_e}$. Plasma-wave excitation by a negatively charged driver has been well studied both theoretically (Esarey *et al.*, 2009; Wilks *et al.*, 1987; Keinigs *et al.*, 1987; Rosenzweig, 1987; Krall *et al.*, 1991; Lu *et al.*, 2005) and experimentally (Joshi *et al.*, 2002; Blumenfeld *et al.*, 2007; Kallos *et al.*, 2008). In the linear regime, the plasma wave driven by a positively charged beam is very similar to those by electrons, but only shifted in phase. However, it presents significant differences in the nonlinear regime. A negatively charged driver "blows out" the background electrons while the positively charged one "sucks them in." In the latter case, electrons in plasma are first "sucked-in" toward the propagating axis by the space-charge force, and then continue to move across the beam axis and create a low-density region behind the driver. This induces phase mixing and local plasma frequency increasing (because of the background electron density enhancement on axis), making it more difficult to obtain a clean "bubble". In the highly nonlinear regime, numerical simulations should be relied on to find the optimal beam-plasma parameters for the resonant wakefield generation.

For comparison to the two dimensional (2D) simulations that follows, a 2D model is performed in Cartesian geometry $(x - y)$. A full three-dimensional treatment can be found (Su *et al.*, 1990; Wilks *et al.*, 1987; Keinigs *et al.*, 1987; Rosenzweig, 1987). We consider a proton beam propagating with a velocity $v_b \approx c$ along x direction through uniform plasma. The charge density of the bunch is $\rho_b = \rho_\perp(y)\rho_{//}(\xi)$, where $\xi \equiv x - v_b t$. In the linear regime, the generated longitudinal

https://doi.org/10.1017/S0263034613000293 Published online by Cambridge University Press

electric field can be calculated as (Wilks *et al.*, 1987)

$$E_x(y, \xi) = X'(\xi)Y(y), \tag{1}$$

where

$$X'(\xi) = -4\pi \int_{\xi}^{\infty} d\xi' \rho_{//}(\xi') \cos k_p(\xi - \xi'), \tag{2}$$

and

$$Y(y) = \frac{k_p}{2} \int_{-\infty}^{\infty} dy' \rho_{\perp}(y') e^{-k_p|y-y'|}, \tag{3}$$

where $\rho_{//}$ and $\rho_{\perp}$ are the longitudinal and transverse charge density profile, and $k_p = \omega_p/c$ is the plasma wave number.

Substitute a Gaussian longitudinal profile $\rho_{//}(\xi) = en_b e^{-\xi^2/2\sigma_x^2}$ into Eqs. (1)–(3), where e is the unit charge of a proton and n_b is the beam density, one obtains the on-axis longitudinal electric field for $\xi \ll -\sigma_x$,

$$E_x(0, \xi) = \sqrt{2\pi}(mc\omega_p/e)(n_b/n_0)(k_p\sigma_x e^{-k_p^2\sigma_x^2/2}) \times Y(0) \cos(k_p\xi). \tag{4}$$

The amplitude of longitudinal electric field peaks when its derivation on k_p is zero, thus giving the match condition of $k_p\sigma_x = \sqrt{2}$ in one-dimensional limit, where $\rho_{\perp} = 1$ for $y = 0$ and remains close to unit for y much larger than k_p^{-1}. The match condition means that the plasma wavelength shall be comparable to the length of the driving bunch. The maximum on-axial electric field is then calculated to be $qE_{x,max}/mc\omega_p \approx 1.3n_b/n_0$.

The above discussions are only valid for the linear-fluid regime. Linear theory is applicable when the perturbed density n_1 is much lower than the background density, i.e., $n_1/n_0 \ll 1$, and the normalized electric field is below unit, i.e., $qE_{z,max}/mc\omega_p \ll 1$. That is to say, the peak beam density must be much lower than the background density $n_b/n_0 \ll 1$. In the weak nonlinear region, according to Lu *et al.* (2005), the longitudinal field will still agree with linear theory until n_b increases to be comparable with n_0.

In the nonlinear one-dimensional regime ($k_p\sigma_y \gg 1$), one can examine the wakefield generation by assuming that the drive beam is non-evolving. The beam profile is a function of the coordinate ξ. Using the momentum and continuity equations, the Poisson's equation can be written as (Esarey *et al.*, 2009)

$$k_p^{-2}\frac{\partial^2\phi}{\partial\xi^2} = \frac{n_b}{n_0} + \gamma_p^2\left\{\beta_p\left[1 - \frac{1}{\gamma_p^2(1+\phi)^2}\right]^{-\frac{1}{2}} - 1\right\}, \tag{5}$$

where ϕ is the normalized electrostatic potential $\phi = e\Phi/mc^2$, $\gamma_p = (1 - \beta_p^2)^{-1/2}$, $\beta_p = v_p/c$ is the phase velocity of the plasma wave that equals the speed of drive proton beam in this case, n_b is the beam density, and n_0 is the background plasma density.

We can see from Eq. (5) that evolvement of wakefield potential ϕ as a function of $k_p\xi$ will not change as long as n_b/n_0 is kept constant. The peak value of ϕ is the same. The only difference is that for lower plasma density n_0, the wakefield potential ϕ evolves slower with ξ, since k_p becomes smaller in this case. As a result, the accelerating field $E_z \sim \partial\phi/\partial\xi$ decreases with n_0 accordingly.

According to this relationship, we consider a Gaussian beam with following parameters (for comparison with the 2D simulations which follow, we proceed with the analysis in 2D Cartesian geometry): The drive beam with beam density n_{b1}, longitudinal size σ_{x1}, radius σ_{y1}, energy γ_1, longitudinal momentum spread ε_1, and divergence angle α_1. The uniform background plasma is of density n_1. To find out the scaling law, one could decrease the background plasma density to $n_2 = 0.01n_1$. According to Eq. (5), the beam density should to be $n_{b2} = 0.01n_{b2}$ to keep similar wakefield evolvement. The match condition ($k_p\sigma_x = \sqrt{2}$) requires $\sigma_{x2} = 10\sigma_{x1}$ (and accordingly $\sigma_{y2} = 10\sigma_{y1}$ to keep the shape of the drive beam). Other parameters stay the same. The wakefield potentials are with the same peak value but evolves 10 times slower with ξ in the latter case, leading to wakefield 10 times smaller. As a result, the accelerating distance should be ten times longer to obtain the same energy gain.

One should notice the beam density in 6d phase space $d \propto N/(\gamma^2\sigma_x\varepsilon\sigma_y^2\alpha^2)$ is 100 times smaller in the second case than the former. It indicates that the requirement of beam quality could be released if we decrease background plasma density. This scaling is very important as beams with high density in 6d phase space are difficult to be obtained. On the other hand, the plasma density should not be too low to insure the accelerating gradient higher than conventional accelerators. Total beam charge cannot exceed the limit that from in conventional accelerators. This would somehow put a lower limit on the beam quality.

3. STABLE ACCELERATION OF THE SELF-CONFINED PROTON BUNCH

In this section, we consider a proton beam with large 6d phase space density driving a wakefield in a uniform plasma with matched density ($k_p\sigma_x = \sqrt{2}$). With such density, the whole beam could be self-confined by the "plasma lens" effect without extra focusing source. Meanwhile, longitudinally the dense plasma electrons zone at the front edge of the first "bubble" would be pulled into the body of the bunch, shielding the expelling force and letting protons at the beam tail fall into accelerating phase of the wakefield.

According to the scaling discussed in Section 2, it's possible to simulate the universal accelerating process in shorter simulating length and time by using higher-density background plasma and a shorter denser proton beam. As a

https://doi.org/10.1017/S0263034613000293 Published online by Cambridge University Press

primary example, we adopt a short dense proton beam with parameters listed in Table 1. 2D-PIC simulation is performed with code VORPAL (Nieter, *et al.*, 2004) as well as quasi-static PIC code LCODE (Lotov, 2003; 1998). Typical proton energy of 1 TeV is used, which is available in conventional radio frequency accelerators. Due to the limitation on simulation ability, relatively small beam duration and high plasma density are employed to obtain a large acceleration gradient, so that we can see considerable energy gain within much shorter simulation length and time. For proton beams that are available in existing facilities, we also perform a long-distance quasi-static simulation with LCODE using a more realistic proton beam with the same 6d-phase space density as that used before (Caldwell *et al.*, 2009). And the results will be discussed in the next section. Alternately, self-modulation (Kumar *et al.*, 2010; Caldwell *et al.*, 2011; Pukhov *et al.*, 2011; Schroeder *et al.*, 2011) also provides a possibility for long proton beams to excite large accelerating field which will be discussed in Section 5.

The energetic proton bunch enters from the left of the simulation box of size 20 μm × 30 μm containing Li gas. Moving window is adopted for long-distance simulation. And two simulation grid sizes are used in this paper. A more precise one $dx = dy = 4.5 \times 10^{-3}\lambda_p \approx 0.02$ μm is used to give a detail shape of the plasma wave, and a rough one $dx = dy = 4.5 \times 10^{-2}\lambda_p \approx 0.2$ μm to simulate acceleration process over a long distance.

Distribution of the protons and momentum vectors of background electrons after $8\lambda_p$ propagation in plasma are shown in Figure 1a. The snapshots of the driving protons are presented by red dots. One can see that the plasma electrons are "sucked-in" by the space-charge force of the driver, and then continue to move across the beam axis and create a "bubble" structure. As in laser- or electron beam-driven cases, the "bubble" size is at the same order of plasma wavelength. Figure 1b shows the corresponding on-axis electric field of the longitudinal plasma wave. The negative electric field at the very front is the unique feature of plasma wakefield driven by positively charged particles, which does not exist in laser- or electron beam-driving cases.

Table 1. *Parameters in the simulation*

Parameters	Symbols	Values	Units
Protons in drive bunch	N_p	1.15×10^{10}	
Proton Energy	E_p	1	TeV
Initial proton longitudinal size	σ_x	1	μm
Initial proton transverse size	σ_r	2.5	μm
Initial proton longitudinal momentum spread	$\Delta P_x/P_x$	0.06	
Initial proton transverse momentum spread	$\Delta P_y/P_x$	10^{-5}	
Plasma density	n_0	5×10^{19}	cm^{-3}
Plasma wavelength	λ_p	4.47	μm

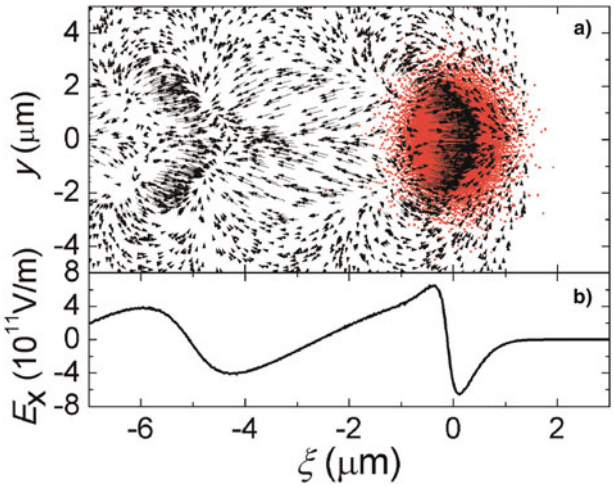

Fig. 1. (Color online) (**a**) Distribution of the protons (red dot) and momentum vector of background electrons (black arrow) after $8\lambda_p$ propagation in plasma. The distribution of the proton beam rarely changes comparing with the original one. (**b**) The corresponding on-axis longitudinal electric field.

The drive bunch we consider here is so dense that space-charge force is large enough to pull the dense electron bulk into the beam body as shown in Figure 1a. Protons located in the beam tail then fall into the accelerating phase of self-excited wakefield. The peak on-axis accelerating gradient shown in Figure 1b reaches approximately 700 GV/m.

However, transverse force in the "bubble" defocuses the accelerated protons. Stable accelerations rely on the balance between the transverse "bubble" field and the effect of co-propagating electrons.

In 2D geometry, consider a particle with charge q moving at the speed of $v_b = \beta c$ along x direction in vacuum, the transverse electromagnetic field at (x, y) is given by

$$E_y = \left\{ \frac{q\gamma(y - y')}{\left[(y - y')^2 + \gamma^2(x - x')^2\right]^{\frac{3}{2}}} \right\}_{ret} \tag{6}$$

$$B_z = \beta E_y \tag{7}$$

where (x', y') is the present position of the charge. As the whole system moves at a velocity very close to the light speed, the retarded effect should be accounted. Figure 2 shows the sketch map. The field at the observation point O is actually originated from the charge located at the retarded position $P^*(x'', y'')$, where $x'' = x' - \beta R$, $y'' = y'$. Here R is the distance from (x'', y'') to the observation point. The subscript "ret" means that the quantity in the brackets is to be evaluated at a retarded time.

When it comes to a charged particle beam with an arbitrary charge density distribution $\rho(x, y)$, Eqs. (6) and (7) are

https://doi.org/10.1017/S0263034613000293 Published online by Cambridge University Press

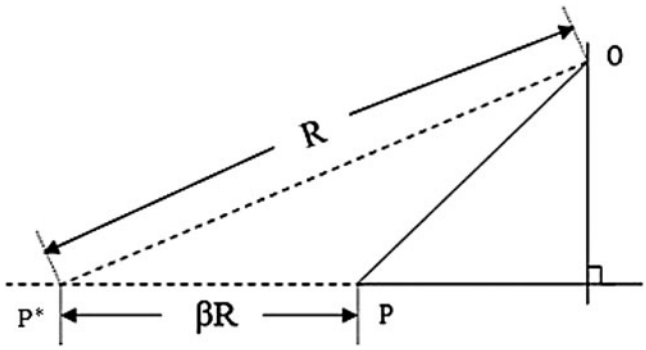

Fig. 2. Sketch map of relativistic retarded effect, P and P* are present and retarded position of the charge, respectively. O is the observation point which has a distance of R from P*.

integrated over the beam region to yield the total field,

$$E_y(\xi, y) = \iint d\xi' dy' \left\{ \frac{\gamma\rho(\xi', y')(y - y')}{\left[(y - y')^2 + \gamma^2(\xi - \xi')^2\right]^{\frac{3}{2}}} \right\}_{\text{ret}}, \quad (8)$$

$$B_z(\xi, y) = \beta E_y(\xi), \quad (9)$$

where $\xi = x - \beta ct$. For a highly relativistic proton bunch $\beta \rightarrow 1$, the space charge force of all the particles in the bunch is balanced by the attractive force due to the self-generated magnetic field. However, when it propagates in a plasma, background electrons will be sucked in and shift with a lower speed compared to the driver. The transverse electric field E_y and magnetic field B_z of these co-propagating electrons are not fully balanced. The general effect $E_y - B_z$ tends to compensate the defocusing transverse wakefield E_{by} in the "bubble" front. The composite transverse force is then

$$F = eW_y + eE_{by} = e(1 - \beta_e) \iint d\xi' dy' \times \left\{ \frac{\gamma\rho(\xi', y')(y - y')}{\left[(y - y')^2 + \gamma^2(\xi - \xi')^2\right]^{\frac{3}{2}}} \right\}_{\text{ret}} + eE_{by} \quad (10)$$

Here $W_y = E_y - B_z$, β_e is the speed of co-propagating electrons normalized by the light speed. We have neglected the electric-magnetic field of the highly relativistic driver since they are almost counteracted ($1 - \beta_b \approx 0$), leaving only the contribution from co-propagating electrons. Transverse electric field in the "bubble" E_{by} can be estimated as (Katsouleas, 1986)

$$E_{by}(\xi, y) = 2E_{x0}(y/k_p a^2) \sin(k_p \xi), \quad (11)$$

where E_{x0} is the maximal longitudinal field amplitude on axis; y satisfies $|y| \leq \sqrt{a^2 - (a + \xi)^2}$, and a is the bubble radius. As ions are assumed to be immobile and the current on the edge of the "bubble" is quite small, additional magnetic field besides B_z is neglected.

Analyzing Eq. (10) relies on the estimation of the co-propagating electrons density $\rho_e(\xi', y')$ and speed β_e. As illustrated in Figures 3a and 3b by PIC simulations, the background electron density peaks near the centre of the driver. The electron density has a symmetric Gaussian-like profile distribution, with the peak density even higher than the beam density.

The density distribution shown in Figures 3a and 3b could be estimated as

$$n_i(\xi, y) = n_{i,\max} \exp\left(\frac{\xi^2}{2\sigma_{ix}^2} + \frac{y^2}{2\sigma_{iy}^2}\right), \quad (12)$$

where i = b or e represents the driver or the co-propagating electrons, respectively. Here σ_{ix} and σ_{iy} are the corresponding longitudinal and transverse length. One can figure out from Figures 3a and 3b that $n_{e,\max} \approx 2.41 n_{b,\max}$, $\sigma_{ex} \approx 0.32\sigma_{bx}$, and $\sigma_{ey} \approx 0.53\sigma_{by}$. In addition, simulations based on different beam-plasma parameters indicate that as the background plasma density n_0 decreases, the proportion of the peak density of co-propagating electrons and the density of the driving proton beam $n_{e,\max}/n_{b,\max}$ tends to increase, while the proportions of length σ_{ex}/σ_{bx} and σ_{ey}/σ_{by} tend to decrease (because the number of co-propagating electrons is limited).

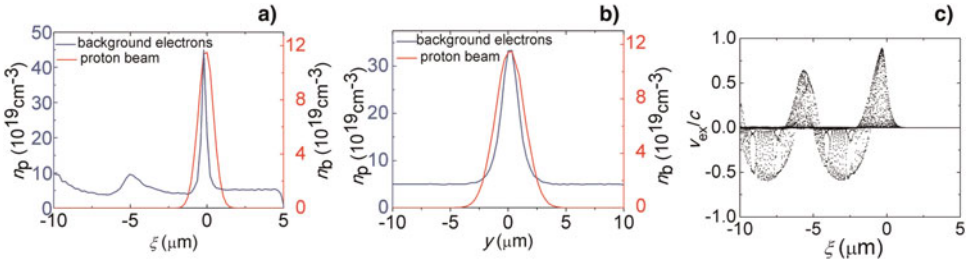

Fig. 3. (Color online) Longitudinal (**a**) and transverse (**b**) density distributions of proton beam (red line) and background electrons (blue line) obtained from PIC simulation. Longitudinal distribution of velocity β_e of the background electrons (**c**).

https://doi.org/10.1017/S0263034613000293 Published online by Cambridge University Press

Substitute Eqs. (11) and (12) to Eq. (10) we obtain the full transverse field as

$$F = e\left\{\iint\left[(1-\beta_e)\frac{\gamma_e q n_e^*(y-y')}{\left[(y-y')^2+\gamma_e^2(\xi-\xi')^2\right]^{\frac{3}{2}}}\right]\right.$$
$$\left. d\xi' dy' + 2E_{x0}\left(\frac{y}{k_p a^2}\right)\sin(k_p\xi)\right\}. \quad (13)$$

where $q = -e$ is the charge of an electron, $\beta_e \approx 0.8$ according to Figure 3c, and $n_e^*(\xi', y') = n_{e,\max}\exp[(\xi'-\Delta)^2/2\sigma_{ex}^2 + y'^2/2\sigma_{ey}^2]$ is the retarded density distribution. The retarded length is $\Delta = \beta_e R$, where R satisfies following relation from Figure 2

$$(1-\beta_e^2)R^2 - 2\beta_e(\xi-\xi')R - [(\xi-\xi')^2 + (y-y')^2] = 0. \quad (14)$$

Combining Eqs. (13) and (14), we obtain the numerical solution with the parameters shown in Table. 1, as presented in Figure 4a.

In order to compare with our analytical results, the wakefield acceleration process is also simulated with the PIC code VORPAL. Our simulation results are presented in Figure 4b. One can see that Figure 4a shows a rough agreement with Figure 4b. The diffractive force of the "bubble" from simulation is slightly larger than expected. This is because Eq. (13) is mainly based on linear theory, where the result is smaller than that in nonlinear situation. This proposed model is relatively simple compared with simulation, but the focusing effect induced by the co-propagating electrons could still be seen in Figure 4a.

In Figure 4c the transverse potential distributions at four typical longitudinal positions are shown,

$$\Psi(y) = -\int_{-\infty}^{y} W(y)dy. \quad (15)$$

The chosen longitudinal positions are marked by dashed curves with corresponding colors in Figure 4d. Well-like structures appear at $y = 0$ for some positions. It is these exhibited potential wells that can confine the proton bunch.

Figure 4d illustrates the on-axis longitudinal electronic field and the distribution of protons and background electrons in the front of "bubble" after 4-cm propagation in the plasma. Comparing with the initial proton beam shape shown in Figure 1a, several important changes have appeared, as discussed below.The well depth at the head of the proton beam ($\xi = 0.5$ μm, the blue curve in Fig. 4c) is much smaller than that in the middle, leading to a weaker confinement. Some protons in this part escape from the well over a few centimeters. Nevertheless most protons in this region propagate stably. One can also find in Figure 4d that protons here are decelerated by the negative electric filed.

The potential well in the middle of the driving bunch ($\xi = 0$ μm, the red curve in Fig. 4c), where most of the co-propagating electrons located, is the deepest among all longitudinal positions. That is why the middle part of the bunch is

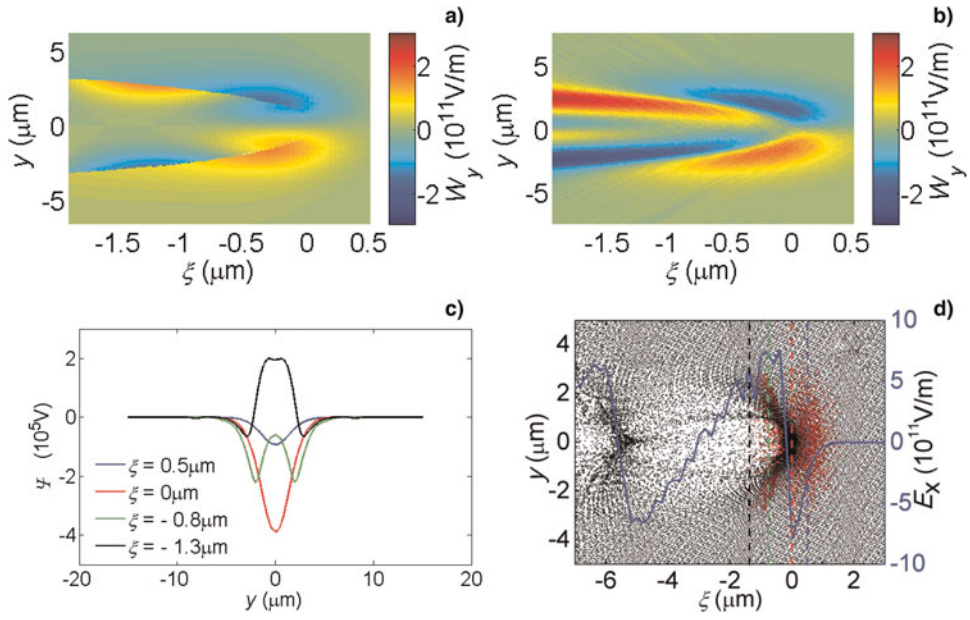

Fig. 4. (Color online) Total transverse field $W(y)$ distributions obtained by numerical calculation (**a**) and PIC simulation (**b**). Transverse potential Ψ as a function of y at different longitudinal positions, $\xi = 0.5$ μm (blue curve), 0 μm (red curve), −0.8 μm (green curve), and −1.3 μm (black curve) from PIC simulation (**c**). (**d**) The on-axis longitudinal electronic field (blue solid), distribution of the beam protons (red dot), background electrons (black dot), and the longitudinal position (marked by corresponding colored dashed) where the potential wells are shown in (**c**).

https://doi.org/10.1017/S0263034613000293 Published online by Cambridge University Press

well confined and narrower (transversely) than other parts as shown in Figure 4d.

At the bunch tail that is close to the co-propagating electrons, the transverse field is still large enough to focus the protons as long as the potential well exists (the peak value in the middle is below zero). The green curve ($\xi = -0.8$ μm) indicates the critical position of the self-confinement. The longitudinal electric field shown in Figure 4d suggests that the protons located between the red dashed and the green dashed, i.e., $-0.8\ \mu\text{m} \le \xi \le 0\ \mu\text{m}$ are not only confined by the self-driving potential well but also efficiently accelerated forward by the positive electric field.

However, for a position far away from the co-propagating electrons ($\xi = -1.3$ μm, black curve in Fig. 4c), the well depth becomes smaller and its shape differs greatly from the one in the middle. The potential at $y = 0$ μm rises up and forms a barrier, expelling protons away from the propagating axis. Therefore, protons in this region tend to be confined in the two small potential wells aside rather than in the middle. All these lead to a "swallow-tail-like" structure in Figure 4d at the bunch tail.

Now we consider the self-confinement condition by placing a test proton in the potential well at transverse position y with a transverse momentum $p_y = \gamma_b v_y$. The proton won't escape from the potential well if its momentum is smaller than the critical value

$$p_y^2 \le p_c^2 \equiv -\frac{\gamma_b q \Psi(y)}{M}, \tag{16}$$

where M is the mass of a proton. So, for a driving bunch with a transverse momentum spread Δp_y, the proportion of protons self-confined in the potential well can be calculated as

$$P = \int_{-y_c}^{+y_c} dy \int_{-p_c}^{p_c} f(y, p_y) dp_y, \tag{17}$$

where $f(y, p_y)$ is the normalized density distribution over transverse coordinate y and momentum p_y with $\iint_{-\infty}^{+\infty} f(y, p_y) dy dp_y = 1$, y_c is the width of the potential well. For the proton bunch in Table 1

$$f(y, p_y) = F(y)G(p_y) = \frac{1}{\sigma_y\sqrt{2\pi}} \times \exp\left(\frac{y^2}{2\sigma_y^2}\right) \frac{1}{\Delta p_y\sqrt{2\pi}} \exp\left(\frac{p_y^2}{2\Delta p_y^2}\right) \tag{18}$$

We obtain $P \approx 1$ and 52.12% for the longitudinal positions of $\xi = -0.8$ μm and -1.3 μm according to the simulation results, respectively, indicating that most protons can be confined.

As analyzed above, protons at the bunch tail experience both an accelerating field and a transverse focusing field. Therefore, these protons can be well confined and accelerated forward. To demonstrate the proposed scheme, a 2D PIC simulation is carried out over an acceleration length as long as one meter.

The evolution of the proton bunch propagating in plasma is shown in Figures 5. Snapshots of the particle phase space (energy versus relative location), are taken at acceleration distances of 0.4 cm, 33 cm, 66 cm, and 1 m. A clear energy transmission from the main body to the protons in the tail is seen. The initial energy of the proton beam is around 1 TeV. As the bunch propagates in the plasma, the main body loses significant amounts of energy, which is picked up by the protons in the beam tail. According to Figures 5c and 5d, one may find that at the later stage of acceleration, the energy gain by the bunch tail grows much slower than in the earlier stage due to the phase slippage effect. It is because the wakefield is "overloaded" by large amounts of protons which lose energy and fall into the accelerating phase. This "overloading" effect actually "pushes" the accelerating phase of the wake back.

The final energy spectrum is compared to the initial one in Figure 6a. After being accelerated for 1 m, the maximal energy of the bunch achieves approximately 1.38 TeV, increasing by 25%. About 4% of the protons gain energy from the rest. The maximum energy as a function of the propagating distance is shown in Figure 6b, where it increases rapidly at the beginning, then much slower after about 80 cm as a result of the de-phasing effect.

4. ACCELERATION OF A PROTON BUNCH WITH LOWER 6D PHASE SPACE DENSITY

According to the scaling relationship discussed in Section 2, if we decrease the background density by 100 times, and change the beam parameters listed in Table 1 according to

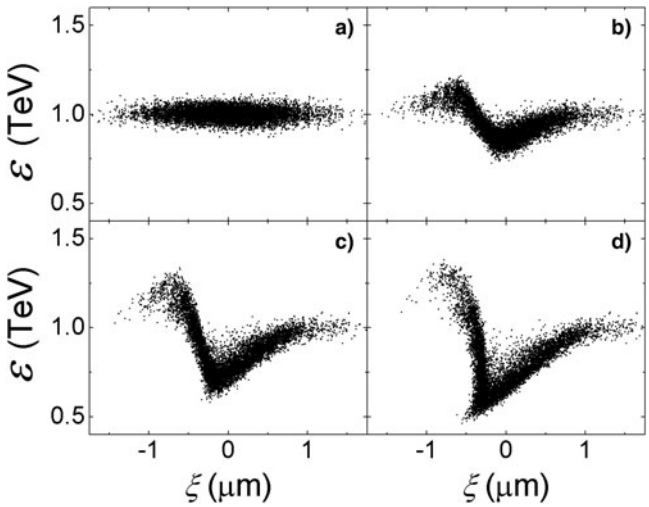

Fig. 5. Phase space (energy versus relative position) of the proton bunch taken at propagating distances of (**a**) 0.4 cm, (**b**) 33 cm, (**c**) 66 cm, and (**d**) 1 m.

https://doi.org/10.1017/S0263034613000293 Published online by Cambridge University Press

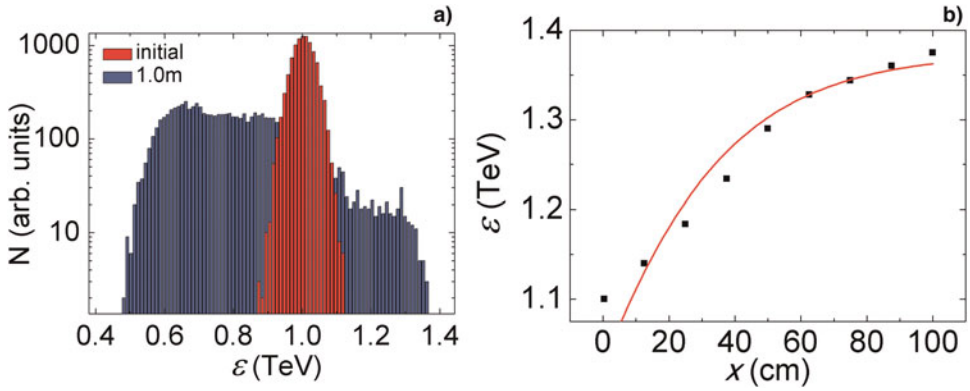

Fig. 6. (Color online) (**a**) Energy spectra of the proton beam at the beginning (red zone) and the end (blue zone) of 1-m propagation in plasma. (**b**) Maximal energy of the protons in the tail of the bunch as a function of the propagating distance, The black dots are obtained from PIC simulation and red solid line is the fitted curve.

the scaling we obtained in Section 2, the total number of particles contained in the beam is then approximately 10^{11}, equaling to that in the LHC beams, while the beam density in 6d phase space $d \propto N/\gamma^2\sigma_x\varepsilon\sigma_y^2\alpha^2$ is approximately 1000 times larger than the LHC beams. For these beam parameters, the whole beam can still be transversely self-confined by co-propagating electrons.

However, for a proton bunch with lower 6d phase space density (like those available in conventional accelerators), if one still keeps the match condition $k_p\sigma_x = \sqrt{2}$, the space charge force is not sufficiently strong to pull the co-propagating electrons into the beam body, and the beam tail won't fall into the accelerating phase of the wakefield. The longitudinal length of the drive beam must be elongated to let an essential part of the beam fall into the accelerating phase. In this situation, the general field induced by the co-propagating electrons can compensate the transverse component of wakefield only in a small area close to the dense electron region. The "plasma lens" effect alone is not strong enough to confine all over the bunch, the head of the beam requires extra guide. We then employ quadrupole magnets with extremely strong field gradients to provide such external focusing field.

The quadrupoles make the beam-plasma interaction essentially three dimensional. However, the effect of quadrupoles can be modeled within the axisymmetric two-dimensional geometry by periodic radial pushes of varying sign given to beam particles (Kudryavtsev *et al.*, 1998). For a sine-like varying field gradient, the time average force acting on the beam is (Lotov *et al.*, 2010)

$$F_q = -\frac{S^2 L_q^2 e^2 r}{8\pi^2 W_p}. \tag{19}$$

where S is the maximum magnetic field gradient, i.e., $B = Sr$, L_q is the space period of the quadrupoles, and W_p is the energy of the protons in the driving bunch. One should note that the focusing force of quadrupole magnets is much smaller than the transverse expelling force in the "bubble." It is only large enough to guide the head of the proton driver, while the accelerated part is still self-confined as we discussed in Section 3.

Here we adopt a proton beam with the same 6d phase space density as that in (Caldwell *et al.*, 2009), but we have elongated the beam (by keeping the longitudinal phase space constant) and changed the radius (by keeping the emittance constant). The parameters are listed in Table 2.

The simulation is performed with the computationally efficient quasi-static code LCODE to achieve acceleration over hundreds of meters. The proton beam density and excited on-axis longitudinal wakefield are shown in Figure 7. One can see the tail of the beam is located in the accelerating phase of the wake, thus the protons there could gain energy from the main body continuously.

As a comparison to Section 3, in Figures 8 and 9, we show the evolution of the proton phase space during propagation and final energy gain, respectively. Here $\xi = 0$ is set to be at the beam head.

The snapshots of the particle phase space (energy versus relative location) in Figure 8 show a very similar acceleration process as that in Figure 5. A proton beam with initial

Table 2. *Parameters in the simulation*

Parameters	Symbols	Values	Units
Protons in drive bunch	N_p	10^{11}	
Proton Energy	E_p	1	TeV
Initial proton longitudinal size	σ_x	150	μm
Initial proton transverse size	σ_r	0.2	mm
Initial proton longitudinal momentum spread	$\Delta P_x/P_x$	0.067	
Initial proton transverse momentum spread	$\Delta P_r/P_x$	6×10^{-5}	
Plasma density	n_0	6×10^{14}	cm^{-3}
Plasma wavelength	λ_p	1.35	mm
Magnetic field gradient	S	0.5	T/mm
space period of the quadrupoles	L_q	3	m

https://doi.org/10.1017/S0263034613000293 Published online by Cambridge University Press

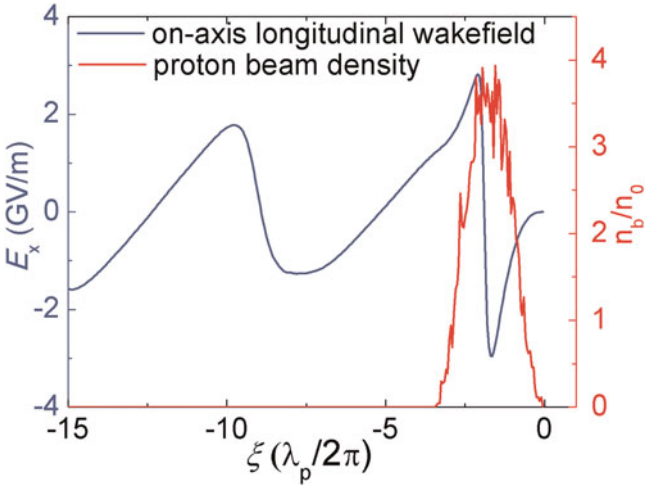

Fig. 7. (Color online) The proton beam density (red curve) and on-axis longitudinal wakefield (blue curve).

energy 1 TeV drives a wakefield in a plasma, which continuously transforms energy from the main body to the protons in the tail. From the energy spectra shown in Figure 9a one can find approximately 4.6% of the protons ($\varepsilon >$ 1.2 TeV) gain energy from the rest. The maximal energy of the bunch reaches 1.5 TeV, increased by 25% compared to the initial peak energy 1.2 TeV, which is very close to the case we discussed in Section 3. We also plot the maximal energy of the protons in the bunch tail versus the propagating distance in Figure 9b. Apparently one can see the energy gain saturates at approximately 320 m because of the phase slippage effect.

5. DISCUSSION

In the plasma-based accelerator, the driver's length should be comparable with the plasma wave length to generate a clean "bubble." For a long proton beam, such as those available in present conventional radio frequency accelerators, the bunch length is generally beyond plasma wave length so that self-modulation will occur. The long relativistic proton bunch will be modulated at the plasma frequency (Kumar *et al.*, 2010; Caldwell *et al.*, 2011) while it can still excite a large amplitude plasma wave. The physical picture of self-modulation instability is similar as in the SMLWFA (self-modulating laser wake field acceleration). When a long bunch of length $L \gg \lambda_p$ propagates in plasmas, it generates a wake within its body, which modulates the bunch in return, leading to a positive feedback. The plasma wave will experience unstable development and tends to modulate the whole beam into micro bunches with length $L' \approx \lambda_p$. These micro bunches then resonantly drive the plasma wake and achieve significant amplitude. A 2D PIC simulation is carried out to verify this effect by varying the proton beam length to $k_p\sigma_z = 28$ (other parameters remain the same as in Table 1). The results are presented in Figure 10. We can see that the driving beam is divided into several micro bunches and forms a bunch chain, with longitudinal length of each bunch comparable to the plasma wavelength.

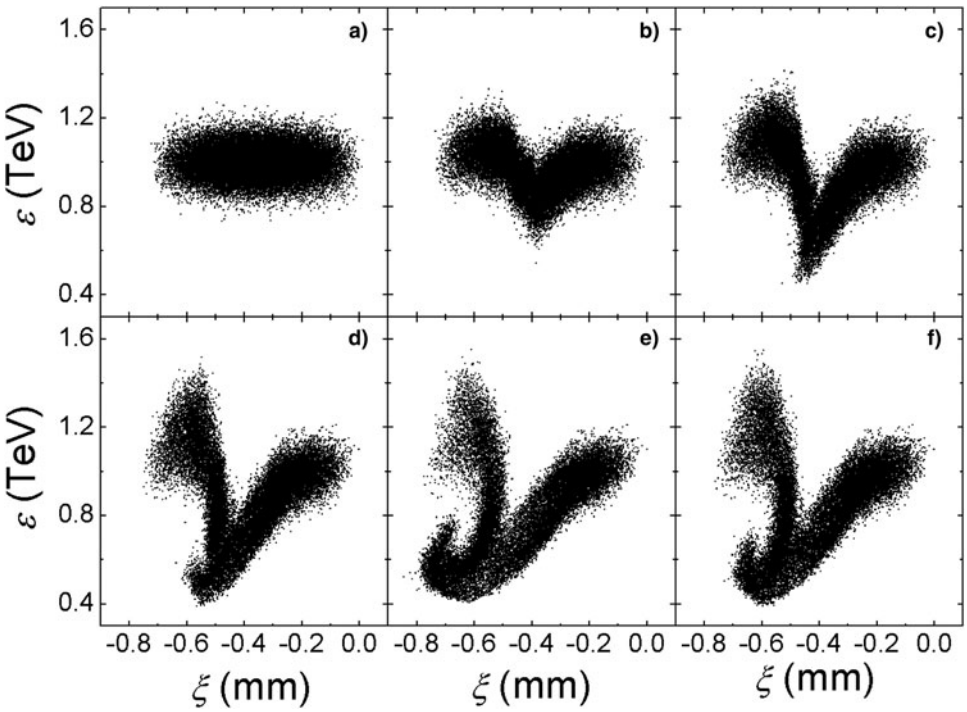

Fig. 8. Phase space (energy versus relative position) of the proton bunch with lower 6d phase-space density taken at propagating distances of (**a**) 0 m, (**b**) 80 m, (**c**) 160 m, (**d**) 240 m, (**e**) 320 m, and (**f**) 400 m.

https://doi.org/10.1017/S0263034613000293 Published online by Cambridge University Press

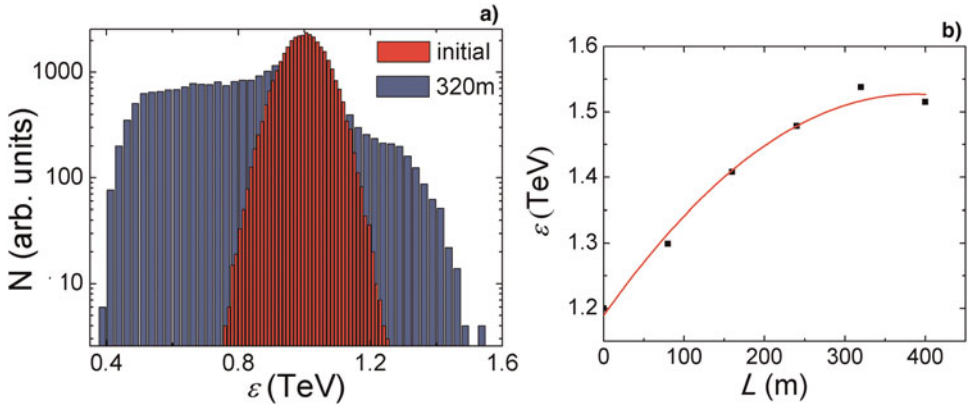

Fig. 9. (Color online) (**a**) Energy spectra of the proton beam at the beginning (red zone) and the after propagating for 320 m in the plasma (blue zone). (**b**) Maximal energy of the protons in the tail of the bunch as a function of the propagating distance, the black dots are obtained from simulation and red solid line is the fitted curve.

After propagating for 4 cm the amplitude of plasma wakefield increases obviously (not shown here). Protons at the tail of each micro bunch tail could gain energy as we have discussed above. However, the bunch train will soon be destroyed by the transverse wakefield as illustrated in Figure 10c, which is harmful for stable acceleration. Several schemes have been proposed to suppress the instability at the micro-bunching stage, such as using a proper longitudinal inhomogeneity of the plasma density (Lotov, 2011). Further research is required to investigate this process. A more detailed discussion on self-modulation instability can be found (Kumar *et al.*, 2010).

Concerning the energy gain of the protons, in both Sections 3 and 4, the peak accelerating field times propagating distance is twice the value of the maximal energy gain of the protons in the bunch tail, i.e., only half of the expected peak value is picked up. This is because only protons located at positions where the plasma lens effect is large enough to compensate the transversely "bubble" field can be accelerated stably, so that only half-peaked acceleration gradient is experienced by these protons. Meanwhile, these protons are so close to the front edge of the "bubble" that they will lose phase soon. To take full advantage of the accelerating field, external injection together with a proton driver with hollow-shaped density distribution (Babu *et al.*, 2011) may be used as an alternative method. Since the beam density peaks on the edge, the transverse field excited by the driver tends to push positively charged particles located at $y < \sigma_y/2$ towards the beam axis, where σ_y is the transverse size of the driver. This kind of transverse field can focus the witnessing protons injected near the beam axis, so that one can inject a witnessing beam at a position where the accelerating field is larger and it experiences a longer acceleration. Detailed research on this acceleration scheme is under consideration.

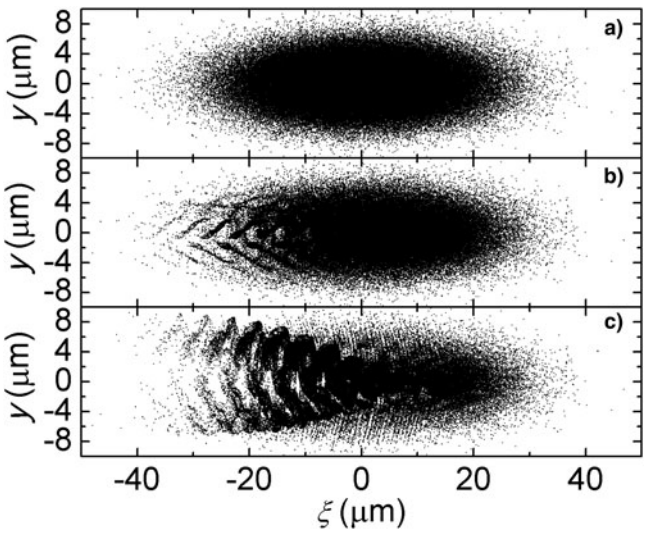

Fig. 10. Proton density distribution at (**a**) 400 um, (**b**) 2 cm, (**c**) 4 cm. The proton beam is of length $k_p\sigma_z = 28$.

6. SUMMARY

In summary, we have proposed that by using a proton beam to drive a plasma wakefield, protons at the tail of the beam can be transversely self-confined and accelerated forward. It is demonstrated that in the front of the "bubble," the transverse field of the co-propagating electrons is large enough to compensate the defocusing effect and focuses the protons in the tail of the bunch. Analysis on the transverse potential well illustrates the self-confinement condition and the evolvement of the beam shape. Two-dimensional simulations on two beams with different 6d phase space densities are performed. In both cases, the peak energy of the self-confined proton beam increases by 25%. This scheme indicates that proton beams available in conventional radio frequency accelerators may gain considerable energy by propagating in an underdense plasma. We also discussed the possibility of using a long proton beam to resonantly drive large amplitude plasma wake due to the self-modulation effect, and a

https://doi.org/10.1017/S0263034613000293 Published online by Cambridge University Press

scheme of using external injection together with a proton driver with a hollow-shaped density distribution to take the full advantage of accelerating field.

ACKNOWLEDGMENTS

This work has been supported by the Ministry of Science and Technology (2011CB808104, 2011DFA11300), National Natural Science Foundation of China (Projects No. 61008010, No. 11125526, No. 11127901, No. 10834008, and No. 60921004).

REFERENCES

Albright, B.J., Yin, L., Bowers, K.J., Hegelich, B.M., Flippo, K.A., Kwan, T.J.T. & Fernandez, J.C. (2007). Monoenergetic and GeV ion acceleration from the laser breakout afterburner using ultrathin targets. *Phys. Plasmas* **14**, 056706.

Albright, B.J., Yin, L., Hegelich, B.M., Bowers, K.J., Kwan, T.J.T. & Fernandez, J.C. (2006). Theory of laser acceleration of light-ion beams from interaction of ultrahigh-intensity lasers with layered targets. *Phys. Rev. Lett*. **97**, 115002.

Babu, P.S., Goswami, A. & Pandit, V.S. (2011). Envelope equations for cylindrically symmetric space charge dominated multi species beam. *Phys. Plasmas* **18**, 103117.

Bane, K.L.F., Chen, P. & Wilson, P.B. (1985). On collinear wake field acceleration. *IEEE Trans. Nuclear Sci*. **NS-32**, 3524–3526.

Blumenfeld, I., Clayton, C.E., Decker, F.J., Hogan, M.J., Huang, C.K., Ischebeck, R., Iverson, R., Joshi, C., Katsouleas, T., Kirby, N., Lu, W., Marsh, K.A., Mori, W.B., Muggli, P., Oz, E., Siemann, R.H., Walz, D. & Zhou, M.M. (2007). Energy doubling of 42 GeV electrons in a metre-scale plasma wakefield accelerator. *Nat*. **445**, 741–744.

Caldwell, A. & Lotov, K.V. (2011). Plasma wakefield acceleration with a modulated proton bunch. *Phys. Plasmas* **18**.

Caldwell, A., Lotov, K, Pukhov, A. & Simon, F. (2009). Proton-driven plasma-wakefield acceleration. *Nat. Phys*. **5**, 363–367.

Chen, M., Pukhov, A., Yu, T.P. & Sheng, Z.M. (2009). Enhanced collimated GeV monoenergetic ion acceleration from a shaped foil target irradiated by a circularly polarized laser pulse. *Phys. Rev. Lett*. **103**, 024801.

Chen, P., Su, J.J., Katsouleas, T., Wilks, S. & Dawson, J.M. (1987). Plasma focusing for high-energy beams. *IEEE Trans. Plasma Sci*. **15**, 218–225.

Davis, J. & Petrov, G.M. (2009). Generation of GeV ion bunches from high-intensity laser-target interactions. *Phys. Plasmas* **16**, 023105.

Eliasson, B., Liu, C.S., Shao, X., Sagdeev, R.Z. & Shukla, P.K. (2009). Laser acceleration of monoenergetic protons via a double layer emerging from an ultra-thin foil. *New J. Phys*. **11**, 073006.

Esarey, E., Schroeder, C. & Leemans, W. (2009). Physics of laser-driven plasma-based electron accelerator. *Rev. Mod. Phys*. **81**, 1229.

Flippo, K., Hegelich, B.M., Albright, B.J., Yin, L., Gautier, D.C., Letzring, S., Schollmeier, M., Schreiber, J., Schulze, R. & Fernandez, J.C. (2007). Laser-driven ion accelerators: Spectral control, monoenergetic ions and new acceleration mechanisms. *Laser Part. Beams* **25**, 3–8.

Gaillard, S.A., Kluge, T., Flippo, K.A., Bussmann, M., Gall, B., Lockard, T., Geissel, M., Offermann, D.T., Schollmeier, M., Sentoku, Y. & Cowan, T.E. (2011). Increased laser-accelerated proton energies via direct laser-light-pressure acceleration of electrons in microcone targets. *Phys. Plasmas* **18**, 056710.

Ji, L.L., Shen, B.F., Zhang, X.M., Wang, F.C., Jin, Z.Y., Li, X.M., Wen, M. & Cary, J.R. (2008). Generating monoenergetic heavy-ion bunches with laser-induced electrostatic shocks. *Phys. Rev. Lett*. **101**, 164802.

Ji, L.L., Shen, B.F., Zhang, X.M., Wang, F.C., Jin, Z.Y., Wen, M., Wang, W.P. & Xu, J.C. (2009). Comment on "generating high-current polarized laser pulse in the phase-stable acceleration regime." *Phys. Rev. Lett*. **102**, 239501.

Joshi, C., Blue, B., Clayton, C.E., Dodd, E., Huang, C., Marsh, K.A., Mori, W.B., Wang, S., Hogan, M.J., O'Connell, C., Siemann, R., Watz, D., Muggli, P., Katsouleas, T. & Lee, S. (2002). High energy density plasma science with an ultrarelativistic electron beam. *Phys. Plasmas* **9**, 1845.

Kallos, E., Katsouleas, T., Kimura, W.D., Kusche, K., Muggli, P., Pavlishin, I., Pogorelsky, I., Stolyarov, D. & Yakimenko, V. (2008). High-gradient plasma-wakefield acceleration with two subpicosecond electron bunches. *Phys. Rev. Lett*. **100**, 074802.

Katsouleas, T. (1986). Physical mechanisms in the plasma wake-field accelerator. *Phys. Rev. A* **33**, 2056–2064.

Keinigs, R. & Jones, M.E., (1987). Two-dimensional dynamics of the plasma wakefield accelerator. *Phys. Fluids* **30**, 252.

Kimura, W.D., Milchberg, H.M., Muggli, P., Li, X. & Mori, W.B. (2011). Hollow plasma channel for positron plasma wakefield acceleration. *Phys. Rev. Spec.Top. Accel. Beams* **14**, 041301.

Krall, J., Joyce, G. & Esarey, E. (1991). Vlasov simulations of very-large-amplitude-wave generation in the plasma wake-field accelerator. *Phys. Rev. A* **44**, 6854–6861.

Kudryavtsev, A.M., Lotov, K.V. & Skrinsky, A.N. (1998). Plasma wake-field acceleration of high energies: Physics and perspectives. *Nucl. Instrum. Meth. Phys. Res. Sect. A* **410**, 388

Kumar, N., Pukhov, A. & Lotov, K. (2010). Self-modulation instability of a long proton bunch in plasmas. *Phys. Rev. Lett*. **104**, 255003.

Lee, S., Katsouleas, T., Hemker, R. & Mori, W.B. (2000). Simulations of a meter-long plasma wakefield accelerator. *Phys. Rev. E* **61**, 7014–7021.

Lee, S., Katsouleas, T., Hemker, R.G., Dodd, E.S. & Mori, W.B. (2001). Plasma-wakefield acceleration of a positron beam. *Phys. Rev. E* **64**, 045501(R).

Liseikina, T.V. & Macchi, A. (2007). Features of ion acceleration by circularly polarized laser pulses. *Appl. Phys. Lett*. **91**, 171502.

Liseykina, T.V., Borghesi, M., Macchi, A. & Tuveri, S. (2008). Radiation pressure acceleration by ultraintense laser pulses. *Plasma Phys. Contr. Fusion* **50**, 124033.

Lotov, K. (2003). Fine wakefield structure in the blowout regime of plasma wakefield accelerators. *Phys. Rev. Spec. Top. Accel. Beams* **6**, 061301.

Lotov, K.V. (1998). Simulation of ultrarelativistic beam dynamics in the plasma wake-field accelerator. *Nucl. Instrum. Methods Phys. Res. Sect. A* **410**, 461–468.

Lotov, K.V. (2007). Acceleration of positrons by electron beam-driven wakefields in a plasma. *Phys. Plasmas* **14**, 023101.

Lotov, K.V. (2010). Simulation of proton driven plasma wakefield acceleration. *Phys. Rev. Spec. Top. Accel. Beams* **13**, 041301.

Lotov, K.V. (2011). Controlled self-modulation of high energy beams in a plasma. *Phys. Plasmas* **18**, 024501.

Lu, W., Huang, C., Zhou, M.M., Mori, W.B. & Katsouleas, T. (2005). Limits of linear plasma wakefield theory for electron or positron beams *Phys. Plasmas* **12**, 063101.

Macchi, A., Cattani, F., Liseykina, T.V. & Cornolti, F. (2005). Laser acceleration of ion bunches at the front surface of overdense plasmas. *Phys. Rev. Lett*. **94**, 165003.

Macchi, A., Veghini, S. & Pegoraro, F. (2009). "Light sail" acceleration reexamined. *Phys. Rev. Lett*. **103**, 085003.

Mora, P. (2003). Plasma expansion into a vacuum. *Phys. Rev. Lett*. **90**, 185002.

Nieter, C. & Cary, J.R. (2004). VORPAL: A versatile plasma simulation code. *J. Comput. Phys*. **196**, 448–473.

Poukey, J.W. (1969). Expansion of a plasma shell into a vacuum magnetic field. *Phys. Fluids* **12**, 1452.

Pukhov, A., Kumar, N., Tuckmantel, T., Upadhyay, A., Lotov, K., Muggli, P., Khudik, V., Siemon, C. & Shvets, G. (2011). Phase velocity and particle injection in a self-modulated proton-driven plasma wakefield accelerator. *Phys. Rev. Lett*. **107**, 145003.

Qiao, B., Zepf, M., Borghesi, M. & Geissler, M. (2009). Stable GeV ion-beam acceleration from thin foils by circularly polarized laser pulses. *Phys. Rev. Lett*. **102**, 145002.

Qiao, B., Zepf, M., Borghesi, M., Dromey, B., Geissler, M., Karmakar, A. & Gibbon, P. (2010). Radiation-pressure acceleration of ion beams from nanofoil targets: The leaky light-sail regime. *Phys. Rev. Lett*. **105**, 155002.

Robinson, A.P.L., Zepf, M., Kar, S., Evans, R.G. & Bellei, C. (2008). Radiation pressure acceleration of thin foils with circularly polarized laser pulses. *New J. Phys*. **10**, 013021.

Rosenzweig, J. (1987). Nonlinear plasma dynanics in the plasma wakefield accelerator. *IEEE Trans. Plasma Sci*. **15**, 186–191.

Rosenzweig, J.B., Breizman, B., Katsouleas, T. & Su, J.J. (1991). Acceleration and focusing of electrons in two-dimensional nonlinear plasma wake fields. *Phys. Rev. A* **44**, R6189–R6192.

Schroeder, C.B., Benedetti, C., Esarey, E., Gruner, F.J. & Leemans, W.P. (2011). Growth and phase velocity of self-modulated beam-driven plasma waves. *Phys. Rev. Lett.* **107**, 145002.

Schwoerer, H., Pfotenhauer, S., Jackel, O., Amthor, K.U., Liesfeld, B., Ziegler, W., Sauerbrey, R., Ledingham, K.W.D. & Esirkepov, T. (2006). Laser-plasma acceleration of quasi-monoenergetic protons from microstructured targets. *Nat*. **439**, 445–448.

Shen, B.F., Li, Y.L., Yu, M.Y. & Cary, J. (2007). Bubble regime for ion acceleration in a laser-driven plasma. *Phys. Rev. E* **76**, 055402.

Shen, B.F., Zhang, X.M., Sheng, Z.M., Yu, M.Y. & Cary, J. (2009). High-quality monoenergetic proton generation by sequential radiation pressure and bubble acceleration. *Phys. Rev. Spec. Top. Accel. Beams* **12**, 121301.

Snavely, R.A., Key, M.H., Hatchett, S.P., Cowan, T.E., Roth, M., Phillips, T.W., Stoyer, M.A., Henry, E.A., Sangster, T.C., Singh, M.S., Wilks, S.C., MacKinnon, A., Offenberger, A., Pennington, D.M., Yasuike, K., Langdon, A.B., Lasinski, B.F., Johnson, J., Perry, M.D. & Campbell, E.M. (2000). Intense high-energy proton beams from petawatt-laser irradiation of solids. *Phys. Rev. Lett*. **85**, 2945.

Su, J.J., Katsouleas, T., Dawson, J.M. & Fedele, R. (1990). Plasma lenses for focusing particle beams. *Phys. Rev. A* **41**, 3321–3331.

Toncian, T., Borghesi, M., Fuchs, J., d'Humières, E., Antici, P., Audebert, P., Brambrink, E., Cecchetti, C.A., Pipahl, A., Romagnani, L. & Willi, O. (2006). Ultrafast laser-driven microlens to focus and energy-select mega-electron volt protons. *Sci*. **312**, 410–413.

Tripathi, V.K., Liu, C.S., Shao, X., Eliasson, B. & Sagdeev, R.Z. (2009). Laser acceleration of monoenergetic protons in a self-organized double layer from thin foil. *Plasma Phys. Controlled Fusion* **51**, 024014.

Wang, X., Muggli, P., Katsouleas, T., Joshi, C., Mori, W.B., Ischebeck, R. & Hogan, M.J. (2009). Optimization of positron trapping and acceleration in an electron-beam-driven plasma wakefield accelerator. *Phys. Rev. Spec. Top. Accel. Beams* **12**, 051303.

Wilks, S., Katsouleas, T., Dawson, J.M., Chen, P. & Su, J.J. (1987). Beam loading in plasma waves. *IEEE Trans. Plasma Sci*. **15**, 210.

Xia, G., Caldwell, A., Lotov, K., Pukhov, A., Kumar, N., An, W., Lu, W., Mori, W.B., Joshi, C., Huang, C., Muggli, P., Assmann, R. & Zimmermann, F. (2010). AIP Conference Proceedings of 14th Advanced Accelerator Concepts Workshop, **1299**, 510–515.

Yan, X.Q., Lin, C., Sheng, Z.M., Guo, Z.Y., Liu, B.C., Lu, Y.R., Fang, J.X. & Chen, J.E. (2008). Generating high-current monoenergetic proton beams by a circularly polarized laser pulse in the phase-stable acceleration regime. *Phys. Rev. Lett*. **100**, 135003.

Yan, X.Q., Wu, H.C., Sheng, Z.M., Chen, J.E. & Meyer-ter-Vehn, J. (2009). Self-organizing gev, nanocoulomb, collimated proton beam from laser foil interaction at 7×10^{21} W/cm^2 (2009). *Phys. Rev. Lett*. **103**, 135001.

Yin, L., Albright, B.J., Hegelich, B.M. & Fernandez, J.C. (2006). GeV laser ion acceleration from ultrathin targets: The laser break-out afterburner. *Laser Part. Beams* **24**, 291–298.

Yin, L., Albright, B.J., Hegelich, B.M., Bowers, K.J., Flippo, K.A., Kwan, T.J.T. & Fernandez, J.C. (2007). Monoenergetic and GeV ion acceleration from the laser breakout afterburner using ultrathin targets. *Phys. Plasmas* **14**, 056706.

Zhang, X.M., Shen, B.F., Ji, L.L., Wang, F.C., Jin, Z.Y., Li, X.M., Wen, M. & Cary, J.R. (2009). Ion acceleration with mixed solid targets interacting with circularly polarized lasers. *Phys. Rev. Spec. Top. Accel. Beams* **12**, 021301.

Zhang, X.M., Shen, B.F., Ji, L.L., Wang, F.C., Wen, M., Wang, W.P., Xu, J.C. & Yu, Y.H. (2010). Ultrahigh energy proton generation in sequential radiation pressure and bubble regime. *Phys. Plasmas* **17**, 123102.

Zhang, X.M., Shen, B.F., Li, X.M., Jin, Z.Y. & Wang, F.C. (2007a). Efficient GeV ion generation by ultraintense circularly polarized laser pulse. *Phys. Plasma* **14**, 123108

Zhang, X.M., Shen, B.F., Li, X.M., Jin, Z.Y. Wang, F.C. & Wen, M. (2007b). Multistaged acceleration of ions by circularly polarzed laers pluse: Monoenergy ion beam generation. *Phys. Plasma* **14**, 073101.

https://doi.org/10.1017/S0263034613000293 Published online by Cambridge University Press